

Computer simulation of impression creep using the hyperbolic sine stress law

Fuqian Yang^a, J.C.M. Li^a, C.W. Shih^b

^a*Department of Mechanical Engineering, University of Rochester, Rochester, NY 14627, USA*

^b*Eastman Kodak Company, Rochester, NY 14652, USA*

Received 15 August 1994

Abstract

Impression creep of materials obeying the Eyring hyperbolic sine constitutive equation is simulated by finite element analysis using the ABAQUS program. It turns out that the impression velocity is also a hyperbolic sine function of the punching stress (the applied load divided by the contact area) and if the punching stress is divided by 3.5 to change to the tension/compression flow stress, the activation shear strain volume calculated from the impression test is the same as that obtained from the tension test. For the same punching stress, the impression velocity is proportional to the punch radius, which is also found in the computer simulation using the power law constitutive equation and by dimensional analysis for both constitutive equations. The present results support the analysis of experimental data of Sn–Pb eutectic alloys reported previously.

Keywords: Computer simulation; Impression creep; Hyperbolic sine stress law

1. Introduction

Impression creep [1–10] is a localized creep test in which a flat-ended cylindrical indenter (also known as a punch) is pressed into the flat surface of a material by a constant load. After a transient stage the indenter moves into the material at a constant velocity. The main advantage of this method is that many tests can be performed on the same sample, avoiding sample-to-sample variations and the use of many samples. The small sample size also makes control of the environment easy to achieve.

Several mechanisms for the impression creep test have been analyzed: bulk diffusion and interface diffusion [1,11], dislocation motion [2,12,13] and viscous flow [14]. By using the finite element method and the von Mises flow rule based on the power law between the strain rate and stress, it was shown that the impression velocity is proportional to the diameter of the indenter and that the relation between the impression velocity and the applied stress obeys the same power law relation as that for uniaxial creep.

Recently, impression test of the Pb–Sn eutectic alloy

[15] were carried out in our laboratory. It was found that the Eyring hyperbolic sine stress law can be used for the relation between the impression velocity and the punching stress in the temperature range 25–110 °C and the stress range 1.5–47 MPa. However, this empirical law cannot be derived by dimensional analysis using the Eyring equation for the elementary interfacial shearing process. Since analytical solutions to the non-linear, elastic–plastic and creep problems do not exist, it is necessary to use the computational approach to analysis of the impression creep test, as done by Yu and Li [2], Hyde et al. [12], and Storakers and Larsson [13] for the power law constitutive equation.

It is the purpose of the present study to analyze in detail the impression creep of the material with Eyring's hyperbolic sine constitutive relation and find the relation between the punching stress and the impression velocity. In the analyses, the following assumptions are made: (1) the material is isotropic and homogeneous, (2) the system is isothermal, (3) the Eyring relation is applicable to each and every element, and (4) the von Mises flow rule is used for three-dimensional plastic flow.

2. Material properties and the boundary value problem

For a material obeying the Eyring relation, the constitutive equation in one dimension is

$$\dot{\varepsilon} = \frac{\dot{\sigma}}{E} + A \sinh(B\sigma) \quad (1)$$

where E , ε and σ are Young's modulus, strain and stress respectively, the dot denotes the time derivative, and A and B are constants. In three dimensions ($\dot{\varepsilon}_{ij}$ and σ_{ij} are the components of the strain rate and stress tensors) the von Mises stress σ_e is used and the corresponding flow rule [16] is

$$\dot{\varepsilon}_{ij} = \frac{1+\nu}{E} \dot{S}_{ij} - \frac{1-2\nu}{E} \dot{P} \delta_{ij} + \frac{3A}{2} \frac{S_{ij}}{\sigma_e} \sinh(B\sigma_e) \quad (2)$$

where ν is the Poisson ratio. The deviatoric stress S_{ij} is

$$S_{ij} = \sigma_{ij} - \frac{1}{3} \sigma_{kk} \delta_{ij} \quad (3)$$

and P and σ_e are

$$P = -\frac{1}{3} \sigma_{kk} \quad (4)$$

$$\sigma_e = \left(\frac{3}{2} S_{ij} S_{ij} \right)^{1/2} \quad (5)$$

From Eq. (2), it is seen that the elastic deformation has no effect on creep at the steady state when \dot{S}_{ij} and \dot{P} are both zero.

In addition the following linear relations are assumed between the strain ε_{ij} and displacement u_i ($i = 1, 2, 3$):

$$\varepsilon_{ij} = \frac{1}{2} \left(\frac{\partial u_i}{\partial x_j} + \frac{\partial u_j}{\partial x_i} \right) \quad (6)$$

and a similar relation between the strain rate $\dot{\varepsilon}_{ij}$ and the velocity \dot{u}_i . Without body forces, the mechanical equilibrium conditions are assumed valid during creep:

$$\frac{\partial \sigma_{ij}}{\partial x_i} = 0 \quad (7)$$

As shown in Fig. 1, the rigid cylindrical indenter is pressed onto the surface of the testing material. The frictionless contact boundary conditions are

$$u_z = h \quad \text{on } S \quad (8)$$

$$\sigma_{rz} = 0 \quad \text{on } S \quad (9)$$

$$\iint_S \sigma_{zz} dS = F \quad \text{on } S \quad (10)$$

where $h = h(t)$ is the impression depth at any time t and $h(0) = 0$, S is the contact area underneath the punch, and F is the applied load. The surface shape outside the contact area is unknown and remains to be determined as part of the analysis.

Over the free surface, the boundary conditions are

$$\sigma_{rz} = 0 \quad \text{on } \bar{S} \quad (11)$$

$$\sigma_{zz} = 0 \quad \text{on } \bar{S} \quad (12)$$

3. Finite element modeling and computation

Earlier computer simulations of impression creep were performed by Yu and Li [2] and Hyde et al. [12], both using the finite element method under the conditions of frictionless contact and the power law constitutive relation for the flow of each element. They used the uniform stress distribution, and the stress distribution due to uniform elastic displacement underneath the punch and the average of the two distributions. Furthermore, they obtained the steady state impression velocity by extrapolating to infinite time.

Our simulation of the impression creep used the large elastoplastic feature of the ABAQUS finite element code. To avoid possible convergence problems arising from the sharp edge of the punch, a rigid punch with a flat end but a round edge ($r/d = 0.002$) was used. The finite element mesh, shown in Fig. 2, consisted of 577 four-node quadrilateral axisymmetric elements and 10 four-node quadrilateral infinite elements and 988 nodes. A linear 2×2 integrating scheme was used. For the large deformation and steep stress gradients at the edge of the contact region, mesh refinement was accomplished around the edge of the contact zone as shown in Fig. 2(b). Along the interface, the interfacial elements IRS21As in the ABAQUS code were used, which automatically monitor the changes in contact area during impressing creep. The displacement as a function of time was obtained directly from the program.

To test the workability of the finite element mesh, elastic impression for the Sn–Pb eutectic alloy, $E = 22$ GPa [17] and $\nu = 0.4$ [18], was performed first. The solutions for the relation between the impression depth and the applied force was compared with results from

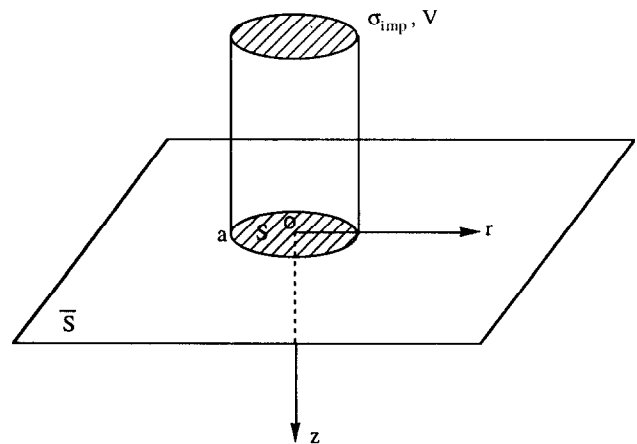


Fig. 1. Impression creep of a half-space.

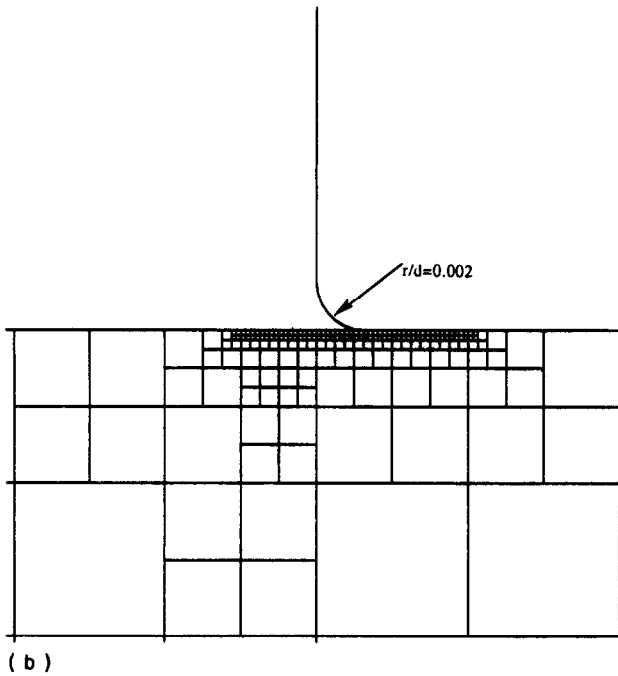
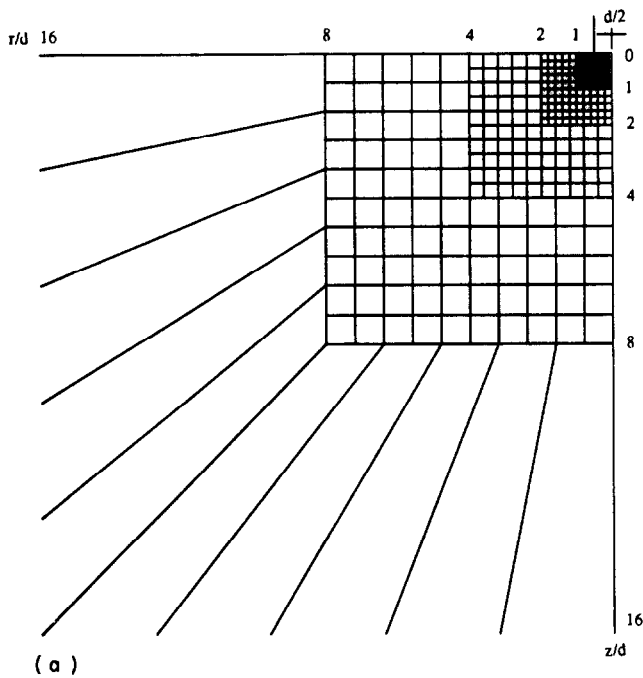


Fig. 2. (a) Finite element mesh for the impression creep of a half-space; (b) refinement mesh around the contact corner.

the analysis of Harding and Sneddon [19] as shown in Fig. 3. It is seen that the agreement is very good. The difference between the Sneddon solution and FEM result is only 0.5% for the depth between $10^{-4}d$ and $10^{-3}d$ and about 3% for the depth between $10^{-3}d$ and $10^{-2}d$ ($d=2a$ is the punch diameter).

Calculation of the impression creep of the material with the Eyring constitutive relation was performed in a Sun-Sparc station 1 with a running time of 25–30 h for an average impression creep experiment at one stress.

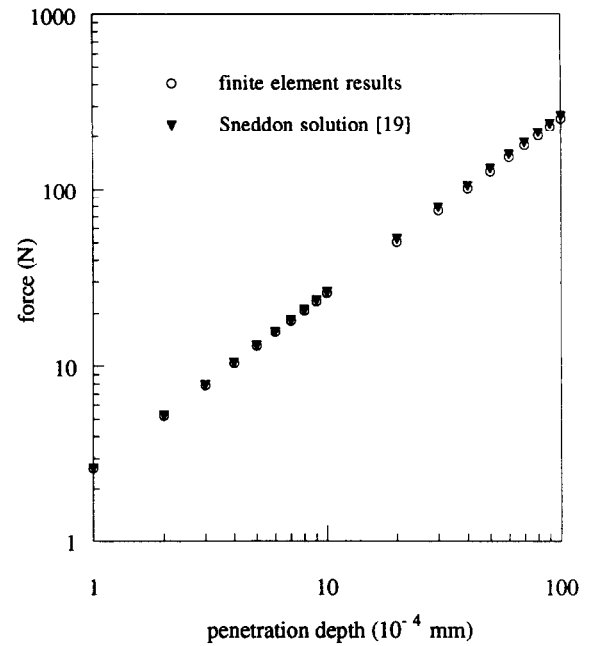


Fig. 3. Comparison of the finite element results with the analytical solution for an elastic impression by a 1 mm punch.

4. Results and discussion

4.1. Numerical parameters, creep curves and deformation of the free surface

To compute the impression velocity, the following (arbitrary) Eyring relation was used for each element in the form of Eq. (1) ($\nu = 0.4$ and $E = 22$ GPa)

$$\dot{\epsilon} = \dot{\sigma}/E + 3.308 \times 10^{-5} \sinh(0.501\sigma) \text{ s}^{-1} \quad (13)$$

where σ is in MPa.

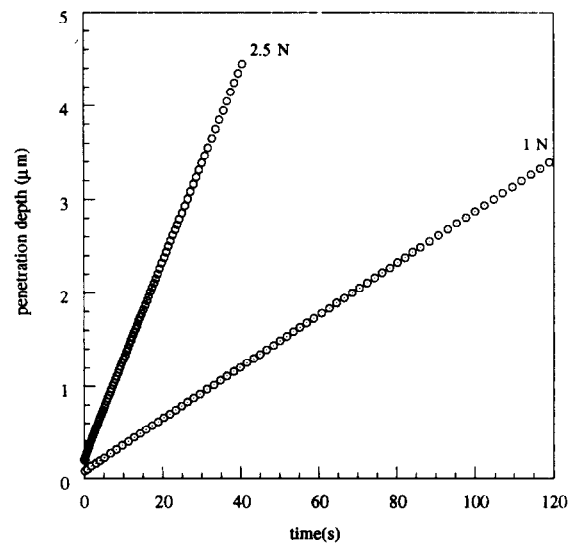


Fig. 4. The penetration depths for a 0.5 mm punch under two punching forces of 1 N and 2.5 N.

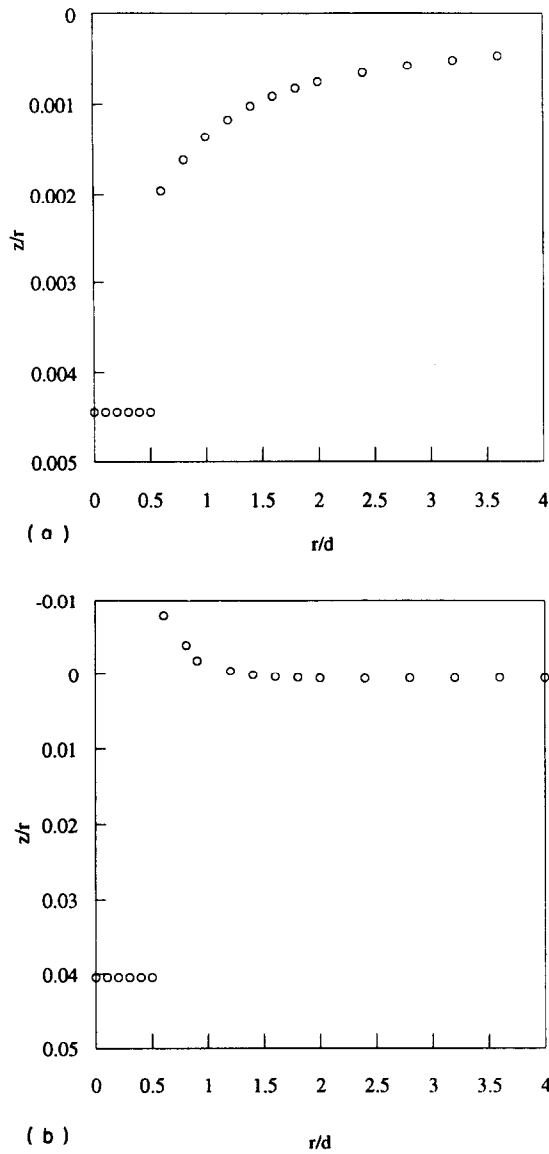


Fig. 5. Surface profile of an impression for the stick boundary condition under a punching load of 8 N over a 0.5 mm punch, (a) at 6.932×10^{-4} s, and (b) at 1.81 s.

A typical penetration depth curve is plotted in Fig. 4, from which it is seen that there is a linear relationship between the penetration depth and the time after a short transient stage. This is in agreement with the experimental observations of the impression creep testing. Fig. 5 shows the shapes of the deformed surface at two penetration times, and the corresponding displacement fields are plotted in Fig. 6. It is seen that there is a pile up of material around the punch for the deeper penetration, and the upward displacement is near the edge of the indenter. It is somewhat surprising that the edge of the indenter can take up so much change of direction and magnitude of the displacement. This pileup of material around the indenter is absent for the linear case [14].

4.2. von Mises stress distribution and its time variation

Since the von Mises stress is the cause of creep, its distribution in the half-space is shown in Fig. 7. It is seen that there is a stress singularity at the edge and a maximum value of von Mises stress at $z/d \approx 0.5$ along the z -axis. Comparing with the von Mises stress distribution for elastic impression [19]

$$\frac{\sigma_e}{\sigma_{\text{imp}}} = \frac{[(7-2\nu)z^2 + (1-2\nu)d^2/4]d^2}{16(z^2 + d^2/4)^2} \quad (14)$$

where σ_{imp} is the punching stress.

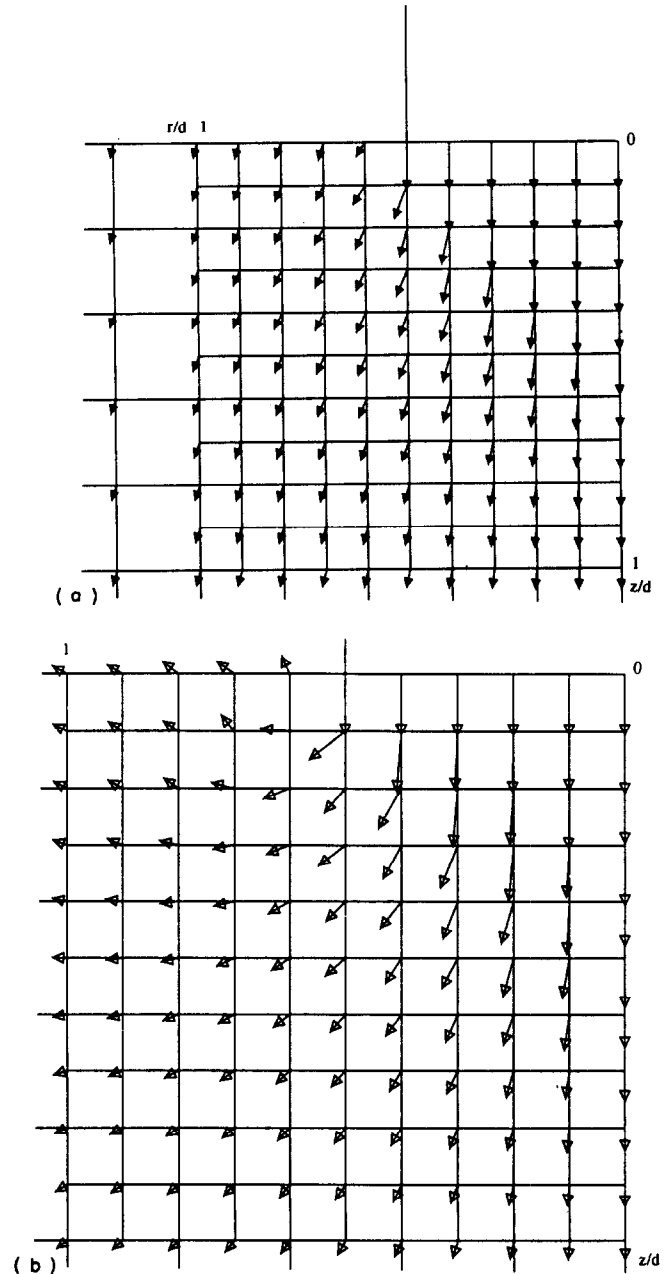


Fig. 6. The displacement field around an impression for the stick boundary condition under a punching load of 8 N over a 0.5 mm punch, (a) at 6.932×10^{-4} s (displacement magnification is 56), and (b) at 1.81 s (displacement magnification is 6).

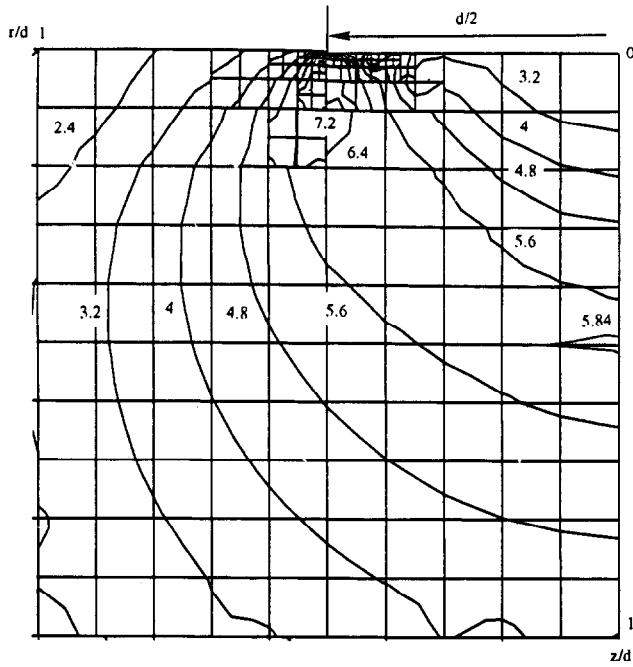


Fig. 7. The von Mises stress distribution for a punching stress of 15.28 MPa and a 0.5 mm diameter punch at a depth of 4.1 μm .

Fig. 8 shows the difference along the z -axis for the same punching stress of 15.28 MPa. It is seen that the distribution is similar but not the same.

Fig. 9 shows the change in von Mises stress with time. At the instant of loading there is a plastic wave propagating in the material which corresponds to the transient stage of the impression creep and after about 5 s the von Mises stress distribution reaches a steady state. It should be mentioned that a finite element

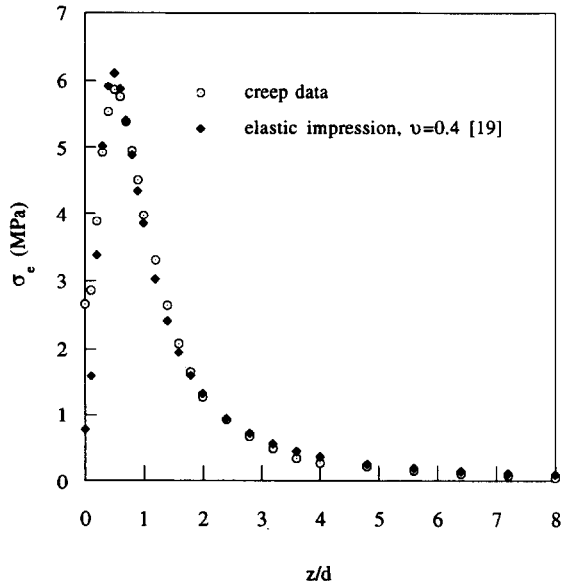


Fig. 8. The von Mises stress distribution along the z -axis for a punching stress of 15.28 MPa and a 0.5 mm diameter punch at a depth of 4.1 μm .

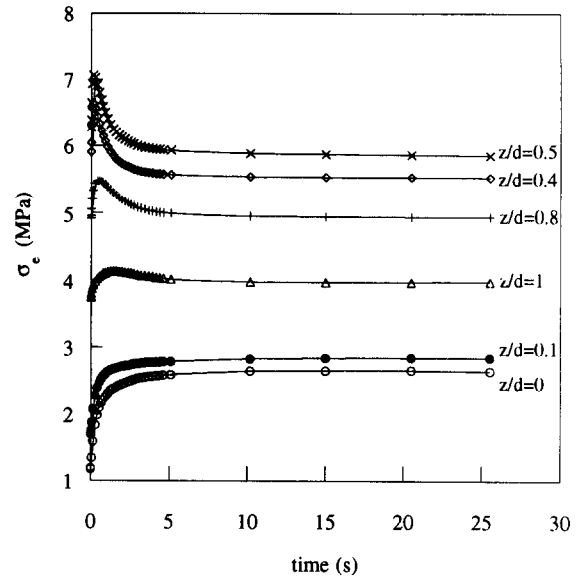


Fig. 9. The von Mises stress along the z -axis at different positions (z/d) plotted as a function of time for a punching stress of 15.28 MPa and a 0.5 mm punch diameter.

calculation on the impact of a rigid punch on an elastic half-space did not show this transient phenomenon. This indicates that it is not due to the elastic wave which will have a transient time of about 0.05 s.

4.3. Stress distribution in the linear case

As mentioned above, the von Mises stress distribution for elastic impression is different from that of creep controlled by the hyperbolic sine law. It is known that Eq. (1) gives a linear relationship between strain rate and stress for small punching stresses, for which an exact stress distribution based on Eq. (2) and using the method in [14] is

$$\sigma_r^c = -\frac{\sigma_{\text{imp}}}{2} \left(J_1^0 - \zeta J_2^0 + \frac{\zeta}{\rho} J_1^1 \right) \quad (15)$$

$$\sigma_\theta^c = -\frac{\sigma_{\text{imp}}}{2} \left(J_1^0 - \frac{\zeta}{\rho} J_1^1 \right) \quad (16)$$

$$\sigma_z^c = -\frac{\sigma_{\text{imp}}}{2} (J_1^0 + \zeta J_2^0) \quad (17)$$

$$\sigma_{rz}^c = -\frac{\sigma_{\text{imp}}}{2} \zeta J_2^1 \quad (18)$$

where

$$\zeta = \frac{z}{a}, \quad \rho = \frac{r}{a} \quad (19)$$

$$J_m^n(\rho, \zeta) = \int_0^\infty k^{m-1} e^{-\zeta k} \sin k J_n(\rho k) dk \quad (20)$$

For elastic impression the stress distribution is [19]

$$\sigma_r^e = -\frac{\sigma_{\text{imp}}}{2} \left(J_1^0 - \zeta J_2^0 - (1-2\nu) \frac{J_0^1}{\rho} + \frac{\zeta}{\rho} J_1^1 \right) \quad (21)$$

$$\sigma_\theta^e = -\frac{\sigma_{\text{imp}}}{2} \left(2\nu J_1^0 + (1-2\nu) \frac{J_0^1}{\rho} - \frac{\zeta}{\rho} J_1^1 \right) \quad (22)$$

$$\sigma_z^e = -\frac{\sigma_{\text{imp}}}{2} (J_1^0 + \zeta J_2^0) \quad (23)$$

$$\sigma_{rz}^e = -\frac{\sigma_{\text{imp}}}{2} \zeta J_2^1 \quad (24)$$

It is seen that the stress distribution for linear plastic deformation is the same as that for elastic impression of incompressible elastic materials ($\nu = 0.5$). The difference shown in Fig. 8 is due to non-linearity in the hyperbolic sine law.

4.4. Effect of rounded edge of the punch, punch radius and mesh size

To examine the influence of the rounded edge on the impression velocity, several round edge radii (r/d of 0.0002 to 0.1) were used for a punching load of 0.1 N, and the impression velocity vs. the edge radius is plotted in Fig. 10. It is seen that, in the range $0.0002d$ – $0.01d$ the round edge has no effect on the steady state impression velocity which increases with an increase in the rounded edge radius $r > 0.01d$.

As shown in Fig. 11, the impression velocity at the same stress is proportional to the punch radius, confirming the dimensional analysis presented before [15].

Owing to the computational limit of the time increment (10^{-60} s) in the ABAQUS code, the maximum $B\sigma$ for this computer simulation is 8.77 for the FEM mesh

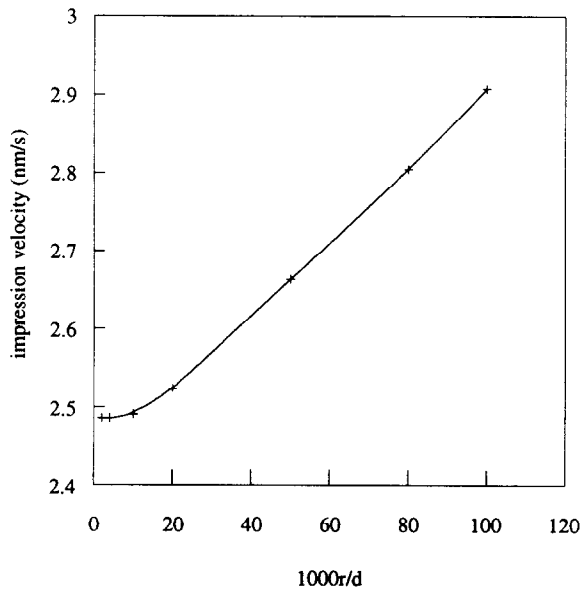


Fig. 10. The effect of the round edge on the impression velocity for a 0.5 mm diameter punch and a punching force of 0.1 N.

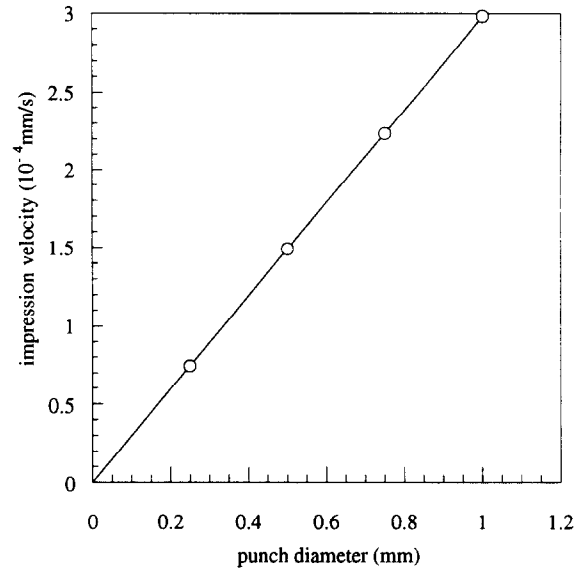


Fig. 11. The effect of the punch diameter on the impression velocity at a punching stress of 15.28 MPa.

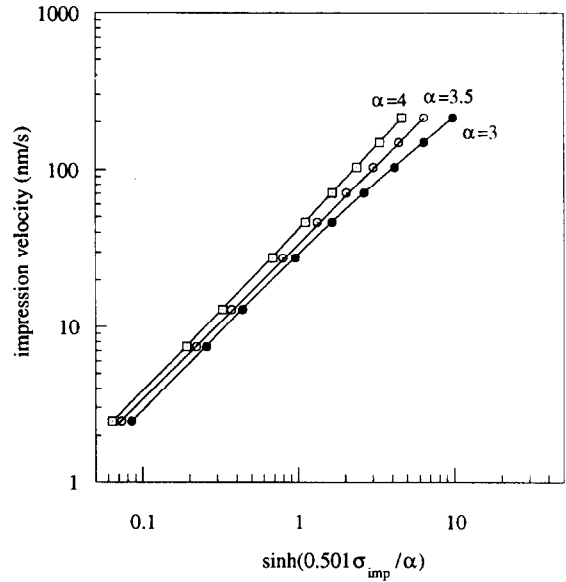


Fig. 12. Effect of α on the velocity–stress relation for a 0.5 mm diameter punch.

shown in Fig. 2. The refinement of mesh dimensions produced an effect on the impression velocity to less than one in the third digit. However, it did produce a decrease in the maximum allowable $B\sigma$.

4.5. Effect of punching stress on the impression velocity

The impression velocity V as a function of punching stress σ_{imp} is shown in Fig. 12 in which V is plotted vs. $\sinh(B\sigma_{\text{imp}}/\alpha)$ for nine different punching stresses between 2.55 and 17.25 MPa or nine different punching loads between 0.5 and 3.5 N for a 0.5 mm diameter punch. The constant α is introduced with the hope that the plot will be straight. It is seen that the plot is indeed

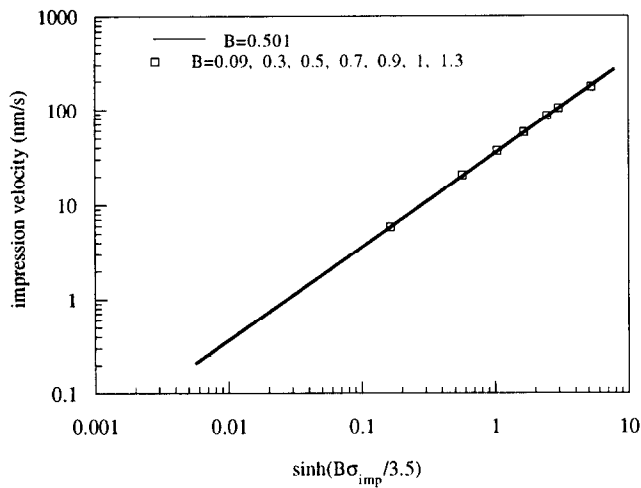


Fig. 13. Effect on B on the impression velocity.

straight for $\alpha = 3.5$ which is similar to the usual number (about 3) used to relate the indentation hardness to the yield stress in tension. This constant 3.50 is good to three digits because 3.49 and 3.51 both give worse standard deviations for the straight line fit on the log-log plot. Furthermore, the slope for the straight line fit for $\alpha = 3.49$ is 0.9995 and that for $\alpha = 3.51$ is 1.0019, so that $\alpha = 3.50$ gives the best straight line with its slope closest to unity. The straight line has the following equation

$$V = \frac{3\pi}{8} aA(3.5) \sinh(B\sigma_{\text{imp}}/3.5) \quad (25)$$

The punch radius a is introduced on account of Fig. 11 and of the dimensional analysis presented before [15]. While this result is expected, it is still surprising to find this equation so similar to the constitutive law, Eq. (13), proposed for each finite element of the material underneath the punch.

This equation reduces to the linear case for small punching stresses for which an analytical solution was obtained using the dual integral equation method because it is exactly the same as the impression creep caused by viscous flow of the material [14]. With this in mind, one can argue that if the impression velocity is proportional to a hyperbolic sine function of punching stress, the relation must be Eq. (25) so it can be reduced to the linear case.

The foregoing observation led us to the suspicion that the validity of Eq. (25) may not depend on the value of B assumed to be 0.501 in the computation. So seven values of B between 0.09 and 1.3 were used for the same punching stress of 25.47 MPa applied to a cylindrical punch of 0.5 mm diameter. The results are shown in Fig. 13 and it is seen that all the points fall on the same line as that shown in Fig. 12 or given by Eq. (25). Here again, although it is somewhat expected, the

result is still a surprise. So we have now convinced ourselves that Eq. (25) is the general relation between impression velocity and the punching stress for any hyperbolic sine constitutive relation applicable to each and every finite element underneath the punch.

A comparison between Eq. (25) for impression creep and Eq. (1) without the elastic term for tensile creep shows

$$\sigma_t = \sigma_{\text{imp}}/3.5 \quad (26)$$

$$\dot{\epsilon} = \frac{16V}{21\pi a} \quad (27)$$

Therefore it is possible to obtain the hyperbolic sine constitutive equation from the impression creep data, provided that the impression velocity also varies with the hyperbolic sine function of punching stress.

This computer simulation thus supports our analysis of Sn–Pb impression creep data reported earlier [15].

5. Summary and conclusions

(1) By using the von Mises flow rule based on Eyring's hyperbolic sine constitutive relation between the strain rate and the tensile stress, computer simulation showed a relation between the impression velocity and the punching stress, Eq. (25). From this equation it is possible to obtain the constitutive relation from the impression creep data and hence the activation shear strain volume for the process.

(2) The results from the computer simulation showed a well defined steady impression velocity with a very small transient stage. For the same punching stress this steady impression velocity was found proportional to the punch diameter, as suggested by the dimensional analysis and confirmed by experiment.

(3) To avoid the stress concentration at the edge of the punch, the edge is rounded and the effect of edge radius on the impression velocity was found negligible when it is less than 1% of the punch diameter.

(4) The von Mises stress distribution during impression creep is somewhat different from that produced elastically by the punch, lower at some places but higher at others. However, for the linear case the stress distribution is the same as that produced by elastic impression, if the Poisson ratio is 0.5.

(5) There is a pile up of material over the peripheral of the impression when the penetration is deep.

Acknowledgements

This work is supported by NSF through grant DMR9221326 which is monitored by Dr. Bruce MacDonald.

References

- [1] S.N.G. Chu and J.C.M. Li, *J. Mater. Sci.*, 12 (1977) 2200.
- [2] H.Y. Yu and J.C.M. Li, *J. Mater. Sci.*, 12 (1977) 2214.
- [3] E.C. Yu and J.C.M. Li, *Philos. Mag.*, 36 (1977) 811.
- [4] G.S. Murty and D.H. Sastry, *Trans. Indian Inst. Met.*, 34 (1981) 195.
- [5] W.S. Gibbs, W.H. Wang, D.K. Matlock and D.L. Oslen, *Welding Res.*, 64 (1985) 153-s.
- [6] Yu.S. Boyarkskay, M.S. Kats and E.I. Purich, *J. Mater. Sci.*, 21 (1986) 1237.
- [7] A. Juhasz, P. Tasnadi, P.S. Zaszvari and I. Kovacs, *J. Mater. Sci.*, 21 (1986) 3287.
- [8] H.Y. Yu, M.A. Imam and B.B. Rath, *Mater. Sci. Eng.*, 79 (1986) 125.
- [9] P.S. Godavarti and K. Linga Murty, *J. Mater. Sci. Lett.*, 6 (1987) 456.
- [10] D. Chiang and J.C.M. Li, *J. Mater. Res.*, 9 (1994) 903.
- [11] F. Yang and J.C.M. Li, *J. Appl. Phys.*, 74 (1993) 4390.
- [12] T.H. Hyde, K.A. Yehia and A.A. Becker, *Int. J. Mech. Sci.*, 35 (1993) 451.
- [13] B. Storakers and P.-L. Larsson, *Royal Institute of Technology, Report 154* (Royal Institute of Technology, Stockholm), 1992.
- [14] F. Yang and J.C.M. Li, unpublished research, 1993.
- [15] F. Yang and J.C.M. Li, *Mater. Sci. Eng.*, A201 (1995) 40.
- [16] *ABAQUS users manual 5.2* (1992), Hibbitt, Karlsson and Sorensen, Inc., Providence, RI, 1992.
- [17] R.E. Pratt, *MS Thesis*, University of Rochester, Rochester, NY, 1991.
- [18] J.H. Lan, D.W. Rice and P.A. Avery, *IEEE Trans. Components Hybrids Manufact. Technol.*, 10 (1987) 346.
- [19] J.W. Harding and I.N. Sneddon, *Proc. Cambridge Philos. Soc.*, 41 (1945) 16.